



Probing the luminescence behavior of Dy³⁺/Eu³⁺ co-doped gadolinium molybdate phosphors under the impact of swift heavy ions

Somrita Dutta^{1,2} · Sudipta Som³ · Mohan Lal Meena⁴ · S. K. Sharma²

Received: 26 January 2024 / Accepted: 23 February 2024 / Published online: 17 April 2024
© The Author(s), under exclusive licence to Springer Science+Business Media, LLC, part of Springer Nature 2024

Abstract

This study delves into the impact of lithium (Li³⁺) and silver (Ag⁷⁺) ion irradiation on the structure and luminescence of Dy³⁺ doped and Dy³⁺/Eu³⁺ co-doped Gd₂MoO₆ phosphors, synthesized via the hydrothermal method. To explore the influence of ions with varied mass and energy, 30 MeV Li³⁺ and 100 MeV Ag⁷⁺ ions were employed at different fluences. We elucidate the induced effects based on defect formation and the role of these ions' linear energy transfer (LET) within the irradiated material. SRIM software estimates the depth profile of the ions. Irradiation of the Gd₂MoO₆ phosphors with Li³⁺ and Ag⁷⁺ ions resulted in the formation of disordered lattices or tracks, modifying their structural, optical, and luminescence properties, which were analyzed by various techniques, including X-ray diffraction, scanning electron microscopy, diffuse reflectance, and photoluminescence. Thermoluminescence (TL) tests and calculations of trapping parameters were conducted to evaluate the dosimetric potential. The findings reveal a more pronounced effect of silver ions compared to lithium ions on the structural and luminescence behavior of doped and codoped Gd₂MoO₆ phosphors due to their higher atomic weight.

Keywords Luminescence · Molybdate · Swift heavy ion · Spectroscopic technique · Depth profile · Linear energy transfer

1 Introduction

Recently, rare earth molybdate materials with the formula R₂MoO₆ (R=rare earth) that have three different types of monoclinic, cubic, and tetragonal polymorphs have drawn the attention of research because of their fascinating luminescent properties due to their stable structure, excellent chemical and thermal stability (Blasse 1968; Chebyshev et al. 2021; Hou et al. 2009). Molybdates are preferred as host materials because they feature a prominent charge transfer band (CTB) in the near-UV or blue spectrum, along with a high quenching concentration of activator ions (Chen and Liu 2013). Due to the low phonon energy of the molybdate host, the introduction of rare earth ions makes these materials promising for dis-

play and lighting applications by enabling high radiative transitions, leading to outstanding luminescence (Chen et al. 2011). Moreover, molybdates offer the advantage of a scalable and cost-effective preparation technique, enhancing their accessibility for various applications. The monoclinic scheelite-type Gd_2MoO_6 structure has previously been investigated as a useful host lattice for rare earth ions (R) due to efficient energy transfer (ET) from the MoO_6^{6-} group to R^{3+} , which aids in efficient photoluminescence emission (Chen et al. 2011). As a result, extensive research with rare earth doped Gd_2MoO_6 phosphors for various color light emissions has been conducted (Huang et al. 2013; Li et al. 2006, 2009). Recent research has investigated the potential of Gd_2MoO_6 doped with Eu^{3+} for fingerprinting applications (Park et al. 2019) and white light-emitting diodes (WLEDs) (Chen et al. 2021). This exploration raises questions about the versatility of these materials beyond LEDs, suggesting that further investigation into their potential applications could be a promising research avenue. To date, there is a lack of adequate experimental or theoretical evidence for the effects of ionizing radiation on Gd_2MoO_6 phosphors. Ionizing radiation is a way to induce extrinsic defects in any material, which can influence its various properties including color emission which is an important point for any phosphor material. One method is to irradiate the materials with Swift heavy ions (SHIs).

The authors have previously demonstrated the effect of SHIs on the structural, optical, and luminescence behavior of undoped Gd_2MoO_6 material (Dutta et al. 2016a, b). It is well known that the basic performance of SHI is mainly focused on material modifications and the development of nanostructures (Kumar et al. 2009) (Mishra et al. 2007), along with the creation of a significant number of defects (Mishra et al. 2007; Avasthi 1997; Mehta 1997). It accelerates various modifications, such as structural, optical and luminescence behaviors of different types of materials (Popov and Balanzat 2000) (Baubekova et al. 2020). The underlying basics related to the irradiation of SHIs and their dependence on the nature of the materials and the energy (Ansari et al. 2021); Ridgway et al. 2011) remain to be established in the case of these phosphor materials.

Keeping this in mind, the present research work aims at investigating Dy^{3+} and Eu^{3+} co-doped Gd_2MoO_6 phosphors for their ion-induced structural, optical, and luminescence behavior compared to their virgin counterparts for the first time using 30 MeV Li^{3+} and 100 MeV Ag^{7+} with different ion fluences. The primary goal in choosing the aforementioned ions for irradiation was to examine the relationship between ions in the periodic table with lower mass and energy and those with higher mass and energy. In order to understand the impact of two different ions in two different parts of the periodic table, the Li ion with a 30 MeV energy has been chosen as the element with the lowest energy, and the 100 MeV Ag ion has been chosen as the element with the highest energy. The ion-induced characteristics are discussed on the basis of the formation of defects concentration and the role of linear energy transfer (LET) of these ion species on this material with ion irradiation. Thermoluminescence (TL) studies and trapping parameters were calculated to explore their dosimetry properties.

2 Materials and methods

The synthesis of Dy³⁺ doped and Dy³⁺/Eu³⁺ co-doped Gd₂MoO₆ and their optimized values have been reported in detail previously (Dutta and Sharma 2016). The SHI irradiation facility was used at the Inter University Accelerator Center, New Delhi. Stopping and Ranging of Ions in Matter (SRIM) software (Stoller et al. 2013) was used to estimate the range of 30 MeV Li³⁺ and 100 MeV Ag⁷⁺ ions where the ion range was estimated at 66.7 μm and 8.70 μm for the synthesized phosphors, respectively. The width of the pellets was between 66 μm and 8 μm, corresponding to the respective ion irradiations such that ions can pass throughout the pellets, excluding the possibility of the implantation of ions. The irradiation fluences used were 1 × 10¹¹- 1 × 10¹³ ions/cm² of 30 MeV Li³⁺ and 1 × 10¹¹- 5 × 10¹² ions/cm² of 100 MeV Ag⁷⁺. The complete information about SHI irradiation is also reported in our previous study (Li et al. 2006). The structural and morphological characterizations of the pristine and irradiated phosphors were confirmed using X-ray diffraction (XRD) and field effect scanning electron microscopy (FESEM) on a Bruker D8 Focus and a Hitachi S-3400 N, respectively. The elemental analysis was carried out using an energy-dispersive X-ray (EDX) spectrometer from ThermoScientific. The luminescence spectra were recorded by a Hitachi F-2500 fluorescence spectrophotometer. The TL glow curves were obtained at a heating rate of 5 °C/s using a Harshaw TLD reader (model 3500).

3 Results and discussion

3.1 Theoretical analysis

The linear energy transfer (LET) calculated (Table 1) using the SRIM code (Avasthi 1997) was further used to simulate the depth profiles in the SHI (Li³⁺ and Ag⁷⁺) induced Dy³⁺ and Dy³⁺/Eu³⁺ Gd₂MoO₆ phosphors. Since the LET value is higher for Ag ions and the range is smaller as compared to Li ions, the effect of the Ag ion is more superficial than that of the Li ion, which breaches deeper in the phosphor pellets. The width of the phosphor pellets is made smaller than the SHI range so that the ions pass through the material transferring their kinetic energy to the host electrons through electron phonon coupling.

This causes an increase in the material's temperature over its melting point and then sudden quenching transpires, creating different defects inside the material (Hodgson et al. 1980; Peña-Rodríguez et al. 2015; Som et al. 2013). The LET value calculated for the Ag⁷⁺ ion is higher, suggesting a more pronounced effect of disorder in both the doped and co-doped phosphors. The two energy losses as a function of beam energy - the nuclear (Sn) energy

Table 1 Ion impact parameters of Dy³⁺ and Dy³⁺/Eu³⁺ Gd₂MoO₆ phosphors

Phosphor	Ion	LET (keV/μm)	Ion range (μm)	Equivalent dose range
Gd ₂ MoO ₆ :Dy ³⁺	Li ³⁺	285	66.70	6.43 kGy- 643 kGy
	Ag ⁷⁺	20750	08.70	468.2 kGy- 46820 kGy
Gd ₂ MoO ₆ :Dy ³⁺ , Eu ³⁺	Li ³⁺	285	66.69	6.43 kGy- 643 kGy
	Ag ⁷⁺	20760	08.70	468.4 kGy- 46840 kGy

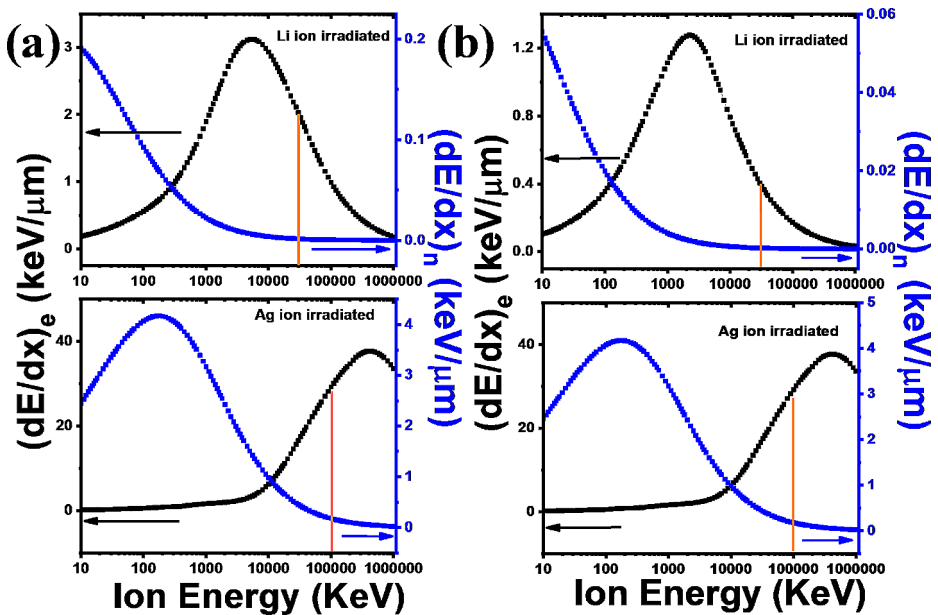


Fig. 1 The Sn and Se of Li and Ag ions irradiated (a) Dy³⁺ (b) Dy³⁺, Eu³⁺ Gd₂MoO₆ phosphors

and electronic (Se) energy losses associated with ion irradiation are shown in Fig. 1 for the irradiated phosphors. Figure 1 shows the variation of Sn and Se as a function of energy for the ion irradiated material. According to the figure, Se outperforms Sn for both doped and co-doped phosphors at energies of 30 MeV and 100 MeV, which correspond to Li ion and Ag ion irradiation, respectively. Thus, in the MeV energy range, Se is responsible for the defects produced and the reordering of the trapping parameters leading to the structural, optical and luminescence modifications in the present materials.

3.2 X-ray powder diffraction (XRD) analysis

Figures 2(a) and 2(b) display the XRD spectra of the irradiated doped and co-doped Gd₂MoO₆ phosphors for the 5×10^{12} ions/cm² ion fluence, respectively with the XRD of the virgin phosphors, indexed according to JCPDS pdf no. 24–0423 (Dutta and Sharma 2016)

The absence of any impurity peak even after high ion fluence irradiation indicates that SHI irradiation has no effect on phase. However, after ion irradiation, the full width at half maximum (FWHM) of Gd₂MoO₆: Dy³⁺ phosphors decreased. The reduction in FWHM seems to contradict the crystalline nature of the sample. This analogous contradictory behavior has been previously documented in studies involving ZnO subjected to irradiation by 100 keV Ne and 1.2 MeV Ar ions (Matsunami N, Sataka M 2003 a b). Generally, polycrystalline host matrices exhibit a high density of defects, with grain boundaries being significantly more defective than the grain interiors (Matsunami N, Sataka M 2003 c). Hence, the reorganization of defects in the grain boundary region during the passage of energetic projectiles is more probable. Therefore, after ion irradiation, the distribution of grain orientation becomes more precise, resulting in a decrease in the FWHM of the XRD

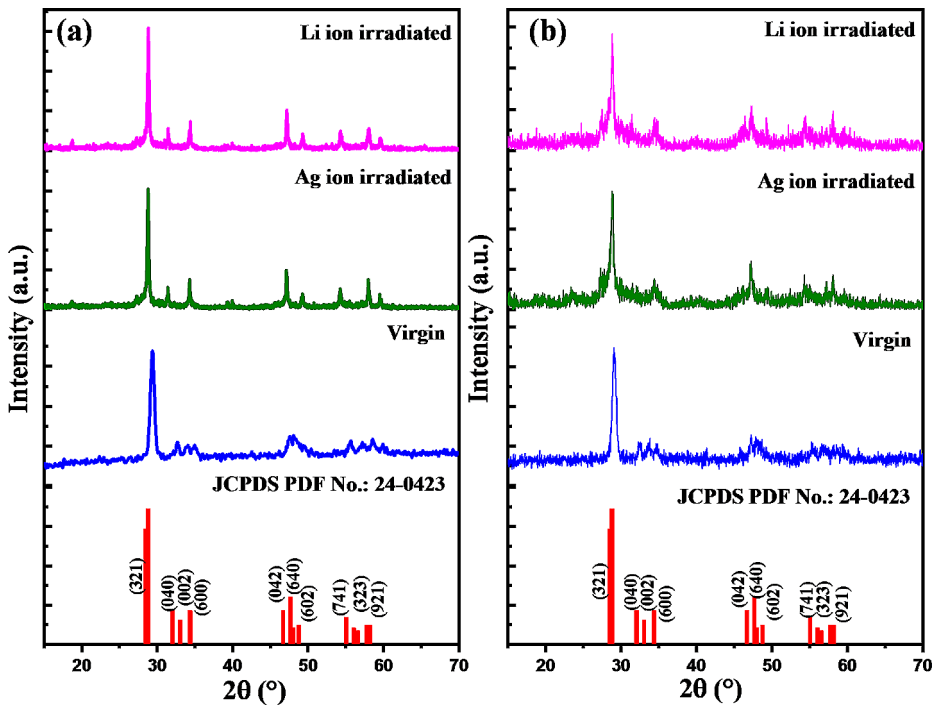


Fig. 2 XRD patterns of ion irradiated (a) Dy³⁺ doped and (b) Dy³⁺/Eu³⁺ co-doped Gd₂MoO₆ phosphors

peak (Matsunami N, Sataka M 2003 b d). However, in the case of Gd₂MoO₆: Dy³⁺/Eu³⁺ phosphors, the FWHM values were observed to increase after ion irradiation. The widening of the XRD peaks shows a reduction in the crystallite size and is also related to the presence of lattice stresses. These non-uniform stresses are caused by the formation of point defects. The energy lost by the high intensity ion beam during the irradiation process causes certain defects, and the crystalline quality worsens with increasing ion dosage (Dutta and Sharma 2016). When compared to the doped phosphor, the co-doped phosphor appeared to be more affected by the ions. This may be attributed to the intensification of already existing defects inside the phosphor because of the co-doping effect of the Eu³⁺ ion.

3.3 FESEM and elemental analysis

Figure 3 depicts the FESEM images of virgin and ion irradiated Dy³⁺ and Dy³⁺/Eu³⁺ phosphors. The fluence rate for Li ion irradiation was used as 1×10^{13} ions/cm², while the ion fluence for Ag ion irradiation was 5×10^{12} ions/cm². FESEM images of the virgin, Li-ion, and Ag-ion irradiated Dy³⁺ doped Gd₂MoO₆ phosphors are shown in Fig. 3 (a-c), respectively

The virgin phosphor shows agglomerated particles. SHI irradiation disrupts the agglomerated particles into irregular particles with reduced sizes. The decrease in particle size might be attributable to the fragmentation of larger grains caused by SHIs irradiation. Similar behavior was observed for Dy³⁺/Eu³⁺ co-doped Gd₂MoO₆ phosphors. Figure 3 (d-f) shows the FESEM images of the virgin, Li ion, and Ag ion irradiated Dy³⁺/Eu³⁺ co-doped

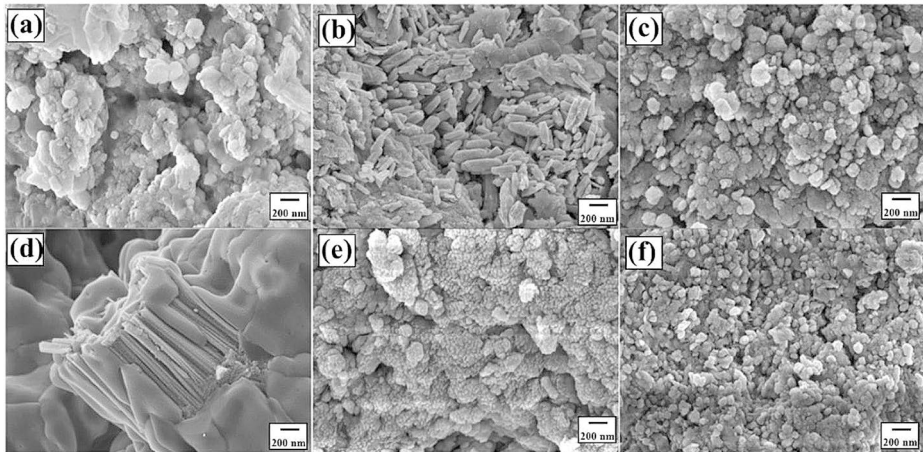


Fig. 3 FESEM images of (a) virgin, (b) Li ion, (c) Ag ion irradiated Dy^{3+} doped Gd_2MoO_6 phosphors, and (d) virgin, (e) Li ion, and (f) Ag ion irradiated $\text{Dy}^{3+}/\text{Eu}^{3+}$ co-doped Gd_2MoO_6 phosphors

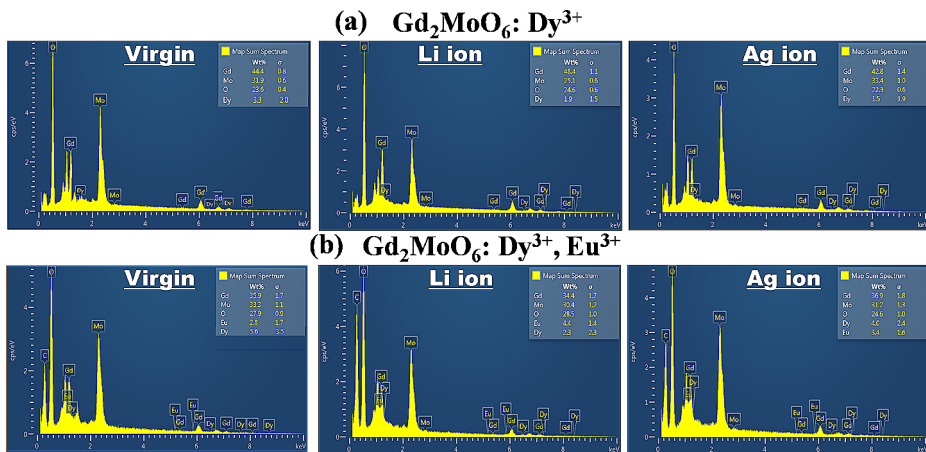


Fig. 4 EDS spectra and elemental composition of the virgin, Li ion and Ag ion irradiated (a) Dy^{3+} doped, and (b) $\text{Dy}^{3+}, \text{Eu}^{3+}$ co-doped Gd_2MoO_6 phosphors. The ion fluence of Li ions, and Ag ions were 1×10^{13} ions/cm² and 5×10^{12} ions/cm², respectively

Gd_2MoO_6 phosphors. The change in size and morphology after ion irradiation is more evident for co-doped Gd_2MoO_6 where the clustered rod like structures (Fig. 3(d)) breaks down to smaller irregular size particles due to the ions (Fig. 3(e-f)) (Dutta et al. 2016a, b). The EDS spectra of the phosphors before and after ion irradiation are shown in Fig. 4 where a, b, c display the doped phosphor and d, e, f exhibit the co-doped $\text{Dy}^{3+}/\text{Eu}^{3+}$ Gd_2MoO_6 . There are no signs of Li or Ag ions in the spectra of b, c, and e, f that ensure irradiation in the virgin doped (a)/ co-doped (d) phosphors, indicating that the ions just transit through the host, causing various forms of defects inside that modify the properties without structurally and chemically changing the materials (Hodgson et al. 1980).

Fig. 5 DR spectra of unirradiated doped and co-doped Gd₂MoO₆ phosphors and inset comparative DR spectra of ion irradiated (a) doped and (b) co-doped Gd₂MoO₆ phosphors

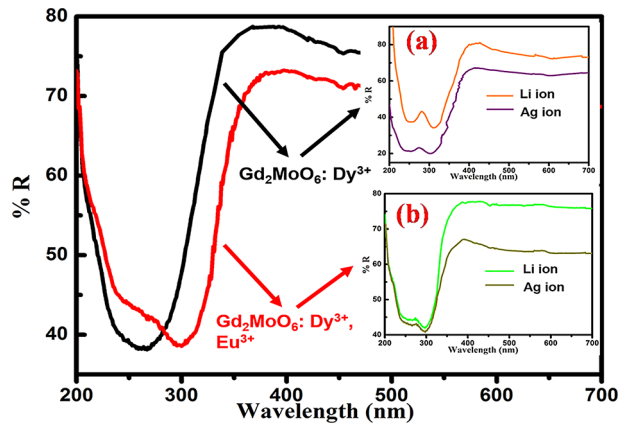
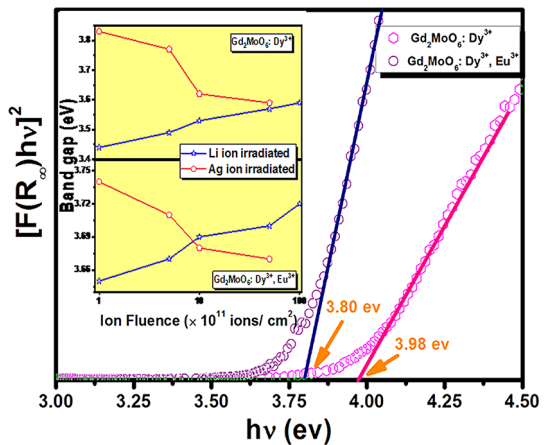


Fig. 6 $[F(R_{\infty})/hv]^2$ vs. hv plot of unirradiated doped and co-doped Gd₂MoO₆ phosphors with band gap values. (Inset) Band gap variation of ion irradiated Gd₂MoO₆ phosphors with varying ion fluences



3.4 Optical characterizations

The comparative diffuse reflectance (DR) spectra of Dy³⁺ and Dy³⁺/Eu³⁺ Gd₂MoO₆ phosphors are shown in Fig. 5. The spectra after irradiation are shown in the inset. The strong band around 260 nm for the doped phosphor can be attributed to the MoO₆⁶⁻ groups and the host charge transfer absorptions (Dong et al. 2014). After Eu³⁺ co-doping, a small shift in the peak with a slight hump around 250 nm is due to the stronger Eu-O charge transfer effect.

After ion bombardment, the DR band demonstrates a prominent distinction with a slight shift in band positions for the Dy doped phosphor as compared to the Eu co-doped phosphor. These alterations are attributed to the ions creating a number of defect states in the phosphors. Also, the reflectance drops for the Ag ion irradiated phosphors, signifying more scattering. The Kubelka-Munk theory (Meena et al. 2022) was used to calculate the band gaps of the phosphors and is shown in Fig. 6. The inset provides the band gap variation with changes in the ion fluences for the two ions. The bandgap of the ion irradiated phosphors decreased when compared to their virgin counterparts, but the variation with ion fluence is

different. The band gap values with increasing ion fluence are given in Table 2. The band gap was observed to decrease slightly with increasing ion fluences for Ag ions. This change in the band gap value might be attributed to structural disorder induced by irradiation and fluence, owing to the high electronic Linear Energy Transfer (LET) of ions [Abu-Hassan, L.H. Townsend 1988–Dutta, S., Som, S., Kunti 2017]. Conversely, the trend in band gap variation differs for Li ion irradiation, showing a slight increase in band gap with Li ion fluence. The lower LET of Li ions as they pass through the molybdate host could be the primary reason for the distinct manifestations of structural disorder and their effects. It is challenging to fully elucidate such phenomena as the impact of heavy ions on any material is multifaceted, and predicting outcomes with certainty is difficult.

3.5 Photoluminescence studies

Figure 7 displays the photoluminescence (PL) spectra of the phosphors before (Fig. 7(a) and (b)) and after ion irradiation (Fig. 7(c) and (d)). In Fig. 7(a) the excitation spectra of the Gd_2MoO_6 phosphors range from 200 to 500 nm recorded for the yellow emission of Dy^{3+} (${}^4\text{F}_{9/2} \rightarrow {}^6\text{H}_{13/2}$ transition) at 577 nm which is the prevailing emission of Dy^{3+} and in Fig. 7 (b) the emission spectra are documented from 400 to 700 nm for an excitation wavelength of 351 nm. The peaks in the excitation spectra centering at 325 nm, 351 nm, 365 nm, 390 nm, 428 nm, 450 nm, and 475 nm are caused by f-f transitions of Dy^{3+} ions corresponding to the (${}^6\text{H}_{15/2} \rightarrow {}^6\text{P}_{3/2}$), (${}^6\text{H}_{15/2} \rightarrow {}^6\text{P}_{7/2}$), (${}^6\text{H}_{15/2} \rightarrow {}^6\text{P}_{5/2}$), (${}^6\text{H}_{15/2} \rightarrow {}^4\text{I}_{13/2}$), (${}^6\text{H}_{15/2} \rightarrow {}^4\text{G}_{11/2}$), (${}^6\text{H}_{15/2} \rightarrow {}^4\text{I}_{15/2}$) and (${}^6\text{H}_{15/2} \rightarrow {}^4\text{F}_{9/2}$) respectively. The two dominant emissions of Dy^{3+} at 488 and 577 nm corresponding to (${}^4\text{F}_{9/2} \rightarrow {}^6\text{H}_{15/2}$) and (${}^4\text{F}_{9/2} \rightarrow {}^6\text{H}_{13/2}$) transitions were further joined by a new peak at 612 nm corresponding to the ${}^5\text{D}_0 \rightarrow {}^7\text{F}_2$ of Eu^{3+} in the co-doped Gd_2MoO_6 phosphor. The detailed study of the co-doping effect on the molybdate phosphor is explained previously (Dutta and Sharma 2016). The fluence used for the comparison was 1×10^{11} ions/cm². Though ion irradiation doesn't affect the PL peak position, the intensity is higher than the virgin one due to the large number of defects created (Abu-Hassan and Townsend 1988; Dutta et al. 2017; Dong et al. 2012)

The response curve with the variation in ion fluence range is viewed in Fig. 8. The PL intensity is affected by the damage caused by SHIs. Primary radiative transitions are indi-

Table 2 Band gap in ion irradiated Gd_2MoO_6 phosphors

Phosphors	Ion fluence (ions/cm ²)	Band gap (eV)	
		Li ion	Ag ion
$\text{Gd}_2\text{MoO}_6: \text{Dy}^{3+}$	Virgin	3.98	
	1×10^{11}	3.44	3.83
	5×10^{11}	3.49	3.77
	1×10^{12}	3.53	3.62
	5×10^{12}	3.57	3.59
	1×10^{13}	3.59	-
$\text{Gd}_2\text{MoO}_6: \text{Dy}^{3+}, \text{Eu}^{3+}$	Virgin	3.80	
	1×10^{11}	3.65	3.74
	5×10^{11}	3.67	3.71
	1×10^{12}	3.69	3.68
	5×10^{12}	3.70	3.67
	1×10^{13}	3.72	-

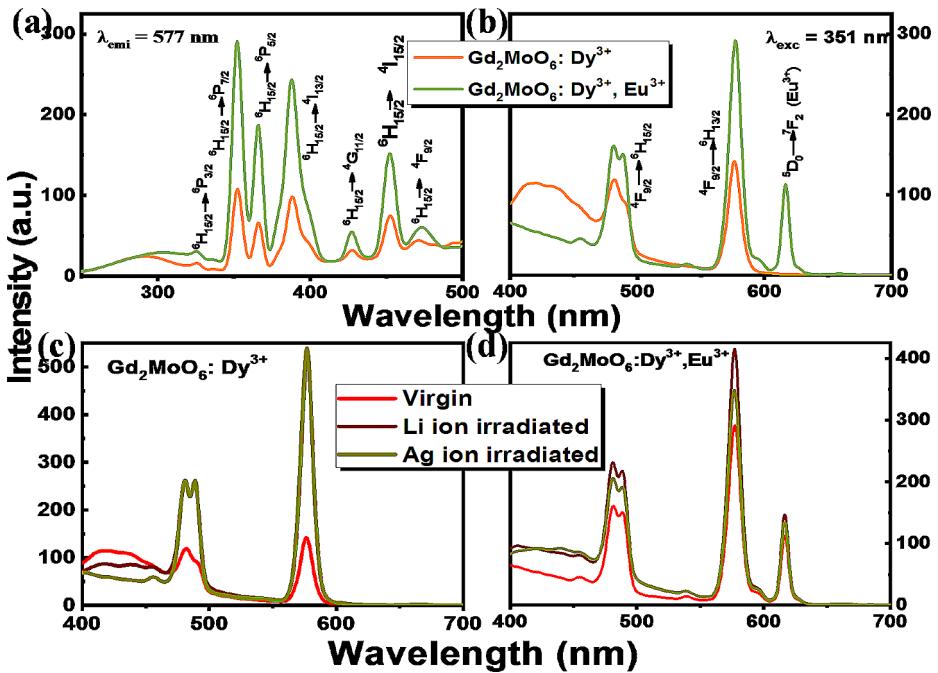
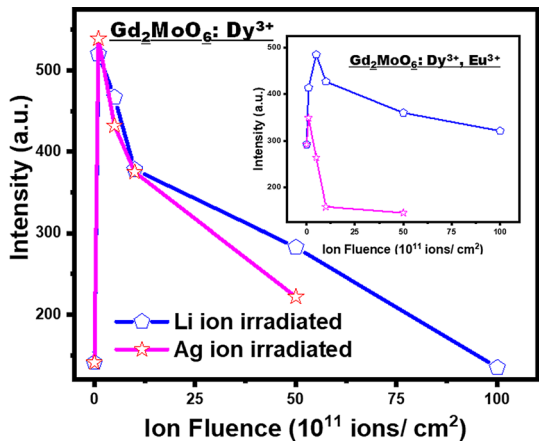


Fig. 7 (a) Comparative PL spectra of doped and co-doped Gd₂MoO₆ phosphors, and comparative PL spectra of (b) doped (c) co-doped Gd₂MoO₆ phosphors before and after ion irradiation

Fig. 8 Dependence of PL intensity of ion irradiated Dy³⁺ doped and (inset) Dy³⁺, Eu³⁺ co-doped Gd₂MoO₆ phosphors with varying ion fluences along with the virgin phosphors (0 fluence)



cated by a high PL intensity. As the concentration of defects acting as color centres grows, the rate of radiative transition also increases. SHI-induced fragmentation increases with SHI fluence, resulting in an increase in defect density or color centers. Thus, the first rise in PL intensities over those of the virgin samples can be attributed to an uptick in defect concentration brought on by ion irradiations. Further, new defects or color centres may develop as a result of an increase in ion fluence (Dutta and Sharma 2016). At a certain ion fluence, these new centres may be annihilated together with the production of luminous quenchers,

which then contribute to the reduction in PL intensity. Therefore, as ion fluence increases, the excitons' energy in the SHI-irradiated phosphors can non-radiatively transfer to the ions' luminous quencher, resulting in a decrease in PL emission intensity.

The color coordinates changes for ion irradiated and virgin phosphors are presented in Fig. 9 (a, d). The color coordinate for the virgin $\text{Gd}_2\text{MoO}_6:\text{Dy}^{3+}$ phosphor is (0.20, 0.26), whereas the CIE coordinate for the virgin $\text{Gd}_2\text{MoO}_6:\text{Dy}^{3+}/\text{Eu}^{3+}$ phosphor is (0.38, 0.30). The color coordinate of virgin $\text{Gd}_2\text{MoO}_6:\text{Dy}^{3+}$ formed mainly due to the presence of two peaks around blue and yellow regions, as shown in Fig. 9 (a). The conjugation of blue to yellow emission can result in a variety of emission colours ranging from blue to near white. In the case of virgin $\text{Gd}_2\text{MoO}_6:\text{Dy}^{3+}$ phosphor, the blue emission intensity was higher than the yellow emission, leading to the color coordinates around the blue region. When the $\text{Gd}_2\text{MoO}_6:\text{Dy}^{3+}$ phosphors were irradiated with Ag and Li ions, the yellow emission intensity increased due to the enhancement of dipole-dipole interaction. Therefore, the emission color shifted towards the white region. The variation of emission coordinates with various ion fluences of Li and Ag is shown in Fig. 9 (b) and (c), respectively.

The brown circle represents the CIE coordinates of the virgin samples. The deep yellow triangle indicates the CIE coordinate of the phosphors irradiated with Li ions having an ion fluence of 5×10^{12} ions/cm². The green cross indicates the CIE coordinate of the phosphors irradiated with Li ions having an ion fluence of 5×10^{12} ions/cm². Furthermore, yellow emission intensity was intensified along with the appearance of another red emission for virgin $\text{Gd}_2\text{MoO}_6:\text{Dy}^{3+}/\text{Eu}^{3+}$ phosphor. The combined emission color was near-white (Fig. 9(d)).

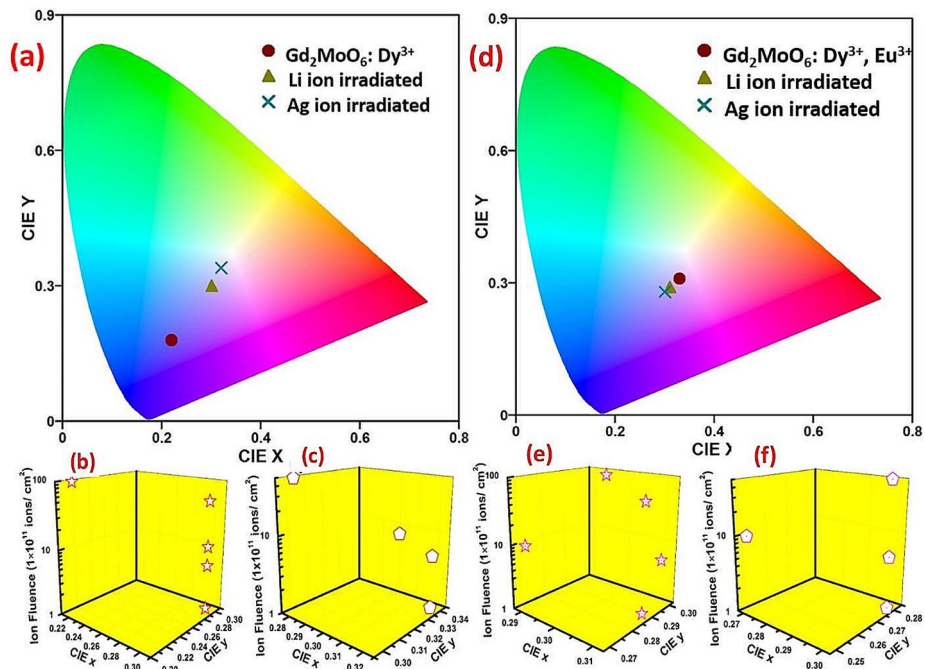


Fig. 9 CIE diagram of (a) doped (d) co-doped Gd_2MoO_6 phosphors before and after ion irradiation. The ion fluence was used as 5×10^{12} ions/cm². The colour coordinates changes of (b, e) Li ion, (c, f) Ag ion irradiated doped and co-doped Gd_2MoO_6 phosphors

When the Gd₂MoO₆: Dy³⁺/ Eu³⁺ phosphors were irradiated with Ag and Li ions, the blue emission intensity increased, and hence the emission coordinate shifted towards the blue region. The variation of emission coordinates with various ion fluences of Li and Ag is shown in Fig. 9 (e-f) respectively.

3.6 Thermoluminescence

3.6.1 TL glow curves analysis

The TL glow curves of Dy³⁺ doped and Dy³⁺/ Eu³⁺ co-doped Gd₂MoO₆ phosphors irradiated with 30 MeV Li³⁺ and 100 MeV Ag ion beam at varying ion fluence range mentioned previously are displayed in Fig. 10. A broad single peak at around 340 °C was found in all instances, but at varying intensities.

For Li ion, with the increase in ion fluence, the intensity of the glow peak of the doped Gd₂MoO₆ phosphor goes on increasing up to the maximum fluence value whereas for the co-doped phosphor the maximum intensity was obtained at 1 × 10¹² ions/cm². When the phosphors are irradiated with Ag ion, 1 × 10¹² ions/cm² was the fluence that produced maximum intensity for the doped phosphor but there was a decrease in intensity from the lowest to the highest fluence for the co-doped one. The first increase and subsequent decrease in

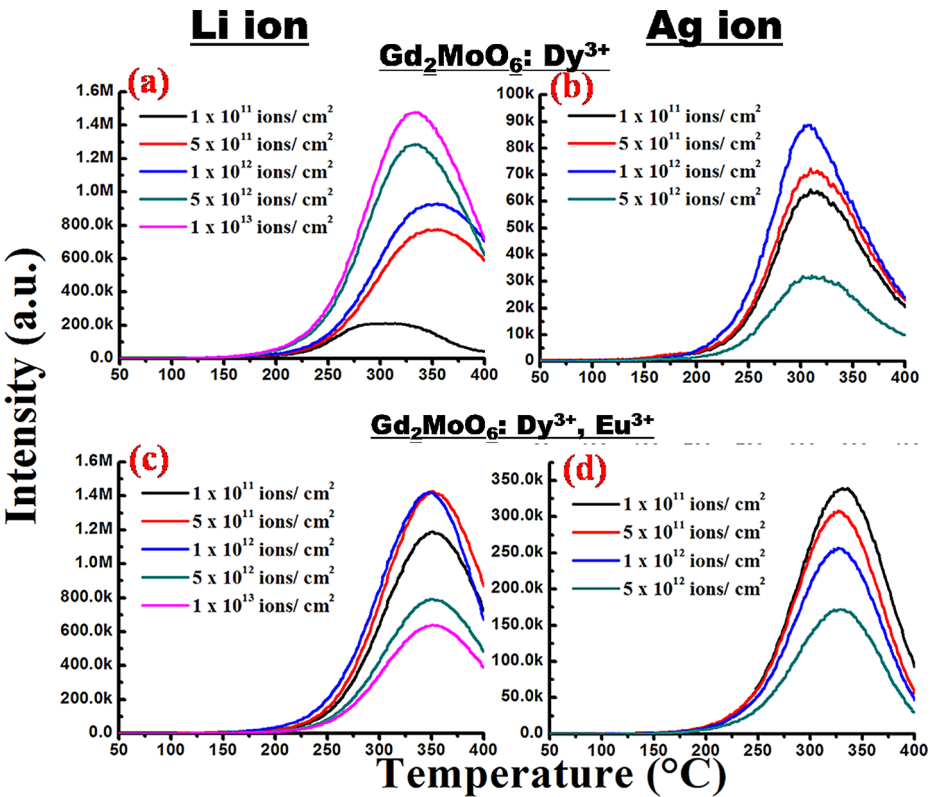


Fig. 10 Comparative TL glow curves of (a, b) Dy³⁺ doped (c, d) Dy³⁺, Eu³⁺ co-doped Gd₂MoO₆ phosphors irradiated with Li and Ag ion respectively with varying ion fluences

TL intensity can be related to a preliminary increase in the quantity of intrinsic traps, as well as lattice disruption at greater fluence caused by strong electronic excitation. For the Ag ion irradiated co-doped Gd_2MoO_6 phosphors the TL intensity decrease can be credited to the lattice disorder effect due to the bulky Ag ion (Atomic Weight=107.868) coupled with the rupture of the O- Mo bonding on the sample surface as well as higher LET value. These inconsistent variations of the TL glow curves can be further clarified by the Track Interaction Model (Horowitz et al. 1996). The TL response curves of the phosphors are shown in Fig. 11.

3.6.2 Trapping parameters

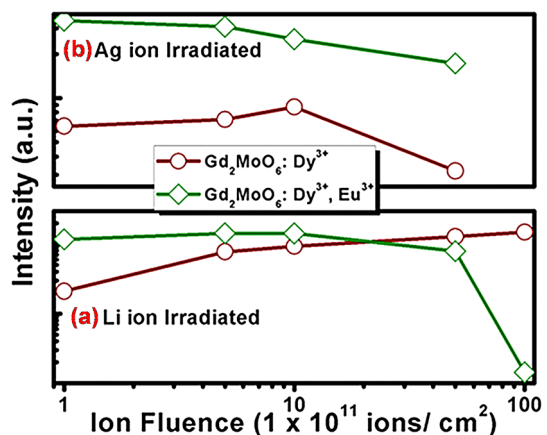
The defects/traps within the material formed after ion irradiation give rise to the TL glow curves. Different trapping parameters divulge the dosimetric behavior of the material after the heavy ions irradiation (Achard et al. 2011). Thermoluminescence glow curves were deconvoluted using the TAnal (Chung et al. 2005) computer program to gain a clear sense of where the traps were located and shown in Fig. 12.

The figure of merit (FOM) determining the quality of fitting was less than 2% for the current study. The kinetic parameters for the deconvoluted peaks were calculated using Chen Formulism (Chen and McKeever 1997); Chen and Winer 1970) and are summarized in Table 3. It was observed that the traps which correspond to the activation energy created for Li ions are less than 1 eV for both the phosphors (0.892 eV and 0.963 eV) whereas for Ag ion irradiated phosphors two peaks were obtained by deconvolution indicating two types of trap centers- one less than 1 eV and another higher. By summing up it can be concluded that when compared to the band gap of the materials, all the trap centers formed are superficial in nature and the deepest trap value is about 1.3 eV for the Ag ion in both the materials.

4 Conclusions

The current investigation reveals that the irradiation of 30 MeV Li^{3+} and 100 MeV Ag^{7+} ions with varying ion fluences is plausible for the creation of disordered lattices or tracks inside the doped and co-doped Gd_2MoO_6 phosphors, which eventually modified their struc-

Fig. 11 Response curves of TL intensity of Dy^{3+} doped and $\text{Dy}^{3+}/\text{Eu}^{3+}$ co-doped Gd_2MoO_6 phosphors with varying ion fluences



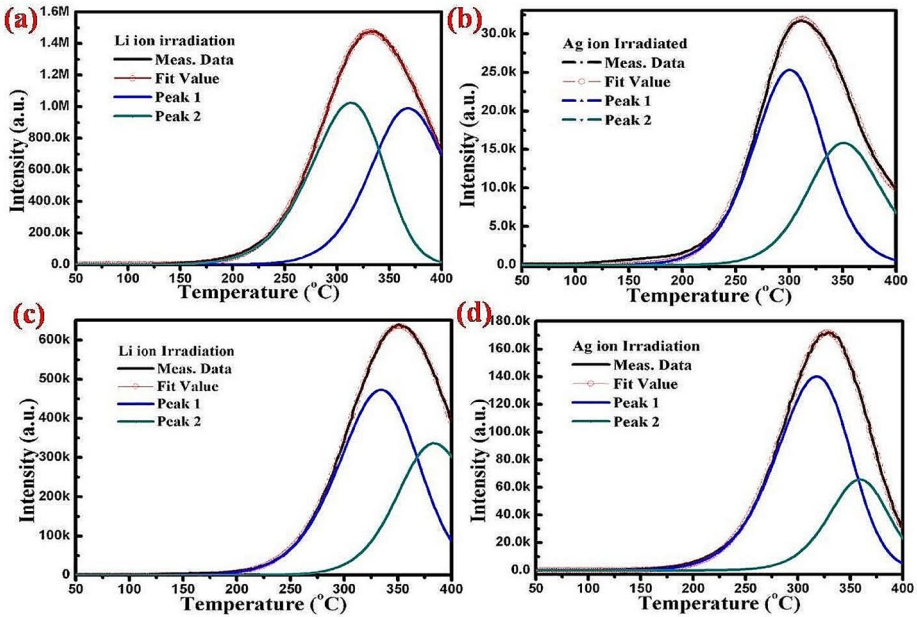


Fig. 12 Deconvolution of TL glow curves for the maximum ion fluence of Li ion, Ag ion irradiated (a, b) Dy³⁺ doped, and (c, d) Dy³⁺/Eu³⁺ co-doped Gd₂MoO₆ phosphors

Table 3 Trapping parameters for doped and co-doped Gd₂MoO₆ phosphors for different ion irradiation

Phosphor	Irradiation type	Peak number	Order of kinetics (b)	Activation energy (E in eV)	Frequency factor (s)
Gd ₂ MoO ₆ : Dy ³⁺	Li	1	1.19	0.892	7.01 × 10 ⁶
	Ag	1	1.45	0.99	8.63 × 10 ⁷
Gd ₂ MoO ₆ : Dy ³⁺ , Eu ³⁺		2	2.00	1.309	7.09 × 10 ⁹
	Li	1	1.3	0.963	1.48 × 10 ⁷
	Ag	1	1.23	0.937	1.56 × 10 ⁷
		2	1.27	1.349	1.11 × 10 ¹⁰

tural, optical, and luminescence properties. Structurally, there is crystallinity loss of the phosphors with the reduction in particle size due to the increment in defect concentration. A decrease in the band gap for both phosphors is observed owing to the structure disorder and defect formation with ion irradiation and fluence. Following ion irradiation, PL peak intensities increased without any corresponding change in peak positions. Thermoluminescence behavior showed a single glow peak for Li ions and two peaks for Ag ions, and a non-linear response in the studied ion fluence range along with superficial traps, which mainly confirm their incompatibility for dosimetry purposes. All the effects were more pronounced for the Ag ion in creating lattice disorder or tracks inside the phosphors due to its bulkier nature and the high electronic LET of the ion.

Acknowledgements Authors are highly thankful to Pelletron group at IUAC, New Delhi, India, for providing ion beam and other facilities.

Author contributions Conceptualization, S.D., S.S., S.K.S.; methodology, S.D.; software, S.D., and M.L.M.; validation, M.L.M., and S.D.; formal analysis, S.D., S.S.; investigation, S.D.; data curation, S.D., and M.L.M.; writing—original draft preparation, S.D., M.L.M.; writing—review and editing, S.S., S.K.S.; All authors have read and agreed to the published version of the manuscript.

Funding This research received no external funding.

Data availability No datasets were generated or analysed during the current study.

Declarations

Conflict of interest The authors declare no conflict of interest.

References

- Abu-Hassan, L.H., Townsend, P.D.: Luminescence Efficiency of Silica during Ion Beam Excitation. *Nucl. Instruments Methods Phys. Res. Sect. B Beam Interact. Mater. Atoms.* **32**, 293–298 (1988). [https://doi.org/10.1016/0168-583X\(88\)90226-1](https://doi.org/10.1016/0168-583X(88)90226-1)
- Achard, P., Adriani, O., Aguilar-Benitez, M., Alcaraz, J., Alemanni, G., Allaby, J., Aloisio, A., Alviggi, M.G., Anderhub, H., Andreev, V.P., et al.: Test of the τ -Model of bose–Einstein correlations and Reconstruction of the source function in Hadronic Z-Boson Decay at LEP. *Eur. Phys. J. C.* **71**, 1648 (2011). <https://doi.org/10.1140/epjc/s10052-011-1648-8>
- Ansari, A.A., Parchur, A.K., Nazeeruddin, M.K., Tavakoli, M.M.: Luminescent Lanthanide nanocomposites in Thermometry: Chemistry of Dopant ions and host matrices. *Coord. Chem. Rev.* **444**, 214040 (2021). <https://doi.org/10.1016/j.ccr.2021.214040>
- Avasthi, D.K.: Role of Swift Heavy ions in materials characterization and modification. *Vacuum.* **48**, 1011–1015 (1997). [https://doi.org/10.1016/S0042-207X\(97\)00114-0](https://doi.org/10.1016/S0042-207X(97)00114-0)
- Baubekova, G., Akilbekov, A., Feldbach, E., Grants, R., Manika, I., Popov, A.I., Schwartz, K., Vasil'chenko, E., Zdorovets, M., Lushchik, A.: Accumulation of Radiation defects and Modification of Micromechanical Properties under MgO Crystal Irradiation with Swift ^{132}Xe ions. *Nucl. Instruments Methods Phys. Res. Sect. B Beam Interact. Mater. Atoms.* **463**, 50–54 (2020). <https://doi.org/10.1016/j.nimb.2019.11.021>
- Blasse, G.: Crystal structure and fluorescence of compounds $\text{Ln}_2\text{Me}^{4+}\text{Me}^{6+}\text{O}_8$. *J. Inorg. Nucl. Chem.* **30**, 2091–2099 (1968). [https://doi.org/10.1016/0022-1902\(68\)80203-9](https://doi.org/10.1016/0022-1902(68)80203-9)
- Chebyshev, K.A., Ignatov, A.V., Pasechnik, L.V., Selikova, N.I., Get'man, E.I.: Investigation of the Heterovalent Substitution Cadmium for Lanthanum in Molybdate La_2MoO_6 . *J. Chem.* 5537048 (2021). <https://doi.org/10.1155/2021/5537048>
- Chen, F., Liu, X.: Structure and Photoluminescence properties of $\text{La}_2\text{Mo(W)O}_6:\text{Eu}^{3+}$ as red phosphors for white LED applications. *Opt. Mater. (Amst).* **35**, 2716–2720 (2013). <https://doi.org/10.1016/j.optmat.2013.08.015>
- Chen, R., McKeever, S.W.S.: *Theory of Thermoluminescence and Related Phenomena*. WORLD SCIENTIFIC, ISBN 978-981-02-2295-6. (1997)
- Chen, R., Winer, S.A.A.: Effects of various Heating Rates on Glow curves. *J. Appl. Phys.* **41**, 5227–5232 (1970). <https://doi.org/10.1063/1.1658652>
- Chen, Y., Wang, J., Liu, C., Kuang, X., Su, Q.: A host sensitized reddish-Orange $\text{Gd}_2\text{MoO}_6:\text{Sm}^{3+}$ phosphor for light emitting diodes. *Appl. Phys. Lett.* **98**, 81917 (2011). <https://doi.org/10.1063/1.3557065>
- Chen, Y., Lan, Y., Wang, D., Zhang, G., Peng, W., Chen, Y., He, X., Zeng, Q., Wang, J.: Luminescence properties of $\text{Gd}_2\text{MoO}_6:\text{Eu}^{3+}$ nanophosphors for WLEDs. *Dalt Trans.* **50**, 6281–6289 (2021). <https://doi.org/10.1039/D1DT00547B>
- Chung, K.S., Choe, H.S., Lee, J.I., Kim, J.L., Chang, S.Y.: A computer program for the deconvolution of Thermoluminescence Glow curves. *Radiat. Prot. Dosimetry.* **115**, 343–349 (2005). <https://doi.org/10.1093/rpd/nci073>

- Dong, N., Yao, Y., Chen, F.: Optical waveguides in nd:GdVO₄ crystals fabricated by Swift N₃+Ion Irradiation. *Opt. Mater. (Amst)*. **35**, 310–313 (2012). <https://doi.org/10.1016/j.optmat.2012.09.024>
- Dong, S., Ye, S., Wang, L., Chen, X., Yang, S., Zhao, Y., Wang, J., Jing, X., Zhang, Q.: Gd₃B(W,Mo)O₉: Eu³⁺ red Phosphor: From structure design to Photoluminescence Behavior and near-UV White-LEDs performance. *J. Alloys Compd.* **610**, 402–408 (2014). <https://doi.org/10.1016/j.jallcom.2014.05.011>
- Dutta, S., Sharma, S.K.: Energy transfer between Dy³⁺ and Eu³⁺ in Dy³⁺/Eu³⁺-Co-doped Gd₂MoO₆. *J. Mater. Sci.* **51**, 6750–6760 (2016). <https://doi.org/10.1007/s10853-016-9962-z>
- Dutta, S., Sharma, S.K., Kumar, V., Som, S., Swart, H.C., Visser, H.G.: Ion-Induced modification of Structural, Optical and luminescence behaviour of Gd₂MoO₆ nanomaterials: A comparative Approach. *Vacuum*. **128**, 146–157 (2016a). <https://doi.org/10.1016/j.vacuum.2016.03.017>
- Dutta, S., Som, S., Kunti, A.K., Sharma, S.K., Kumar, V., Swart, H.C., Visser, H.G.: Ag⁷⁺ Ion Induced modification of morphology, Optical and Luminescence Behaviour of Charge compensated CaMoO₄ Nanophosphor. *Nucl. Instruments Methods Phys. Res. Sect. B Beam Interact. Mater. Atoms.* **384**, 76–85 (2016b). <https://doi.org/10.1016/j.nimb.2016.08.007>
- Dutta, S., Som, S., Kunti, A.K., Kumar, V., Sharma, S.K., Swart, H.C., Visser, H.G.: Structural and luminescence responses of CaMoO₄ Nano Phosphors synthesized by Hydrothermal Route to Swift Heavy Ion Irradiation: Elemental and Spectral Stability. *Acta Mater.* **124**, 109–119 (2017). <https://doi.org/10.1016/j.actamat.2016.11.002>
- Hodgson, R.T., Baglin, J.E.E., Pal, R., Neri, J.M., Hammer, D.A.: Ion Beam Annealing of Semiconductors. *Appl. Phys. Lett.* **37**, 187–189 (1980). <https://doi.org/10.1063/1.91819>
- Horowitz, Y.S., Rosenkrantz, M., Mahajna, S., Yossian, D.: The Track Interaction Model for Alpha Particle Induced Thermoluminescence Supralinearity: Dependence of the Supralinearity on the Vector properties of the alpha particle Radiation Field. *J. Phys. D Appl. Phys.* **29**, 205–217 (1996). <https://doi.org/10.1088/0022-3727/29/1/031>
- Hou, Z., Lian, H., Zhang, M., Wang, L., Lü, M., Zhang, C., Lin, J.: Preparation and Luminescence properties of Gd₂MoO₆:Eu³⁺ nanofibers and nanobelts by Electrospinning. *J. Electrochem. Soc.* **156**, J209 (2009). <https://doi.org/10.1149/1.3138702>
- Huang, M.N., Ma, Y.Y., Huang, X.Y., Ye, S., Zhang, Q.Y.: The Luminescence properties of Bi³⁺ sensitized Gd₂MoO₆:RE³⁺ (RE=eu or sm) phosphors for Solar Spectral Conversion. *Spectrochim Acta Part. Mol. Biomol. Spectrosc.* **115**, 767–771 (2013). <https://doi.org/10.1016/j.saa.2013.06.111>
- Kumar, V., Swart, H.C., Ntwacaborwa, O.M., Kumar, R., Lochab, S.P., Mishra, V., Singh, N.: Thermoluminescence Response of CaS:Bi³⁺ Nanophosphor exposed to 200 MeV ag+15 Ion Beam. *Opt. Mater. (Amst)*. **32**, 164–168 (2009). <https://doi.org/10.1016/j.optmat.2009.06.018>
- Li, G., Wang, Z., Quan, Z., Liu, X., Yu, M., Wang, R., Lin, J.: Sol-Gel Growth of Gd₂MoO₆:Eu³⁺ nanocrystalline layers on SiO₂ spheres (SiO₂@Gd₂MoO₆:Eu³⁺) and their luminescent properties. *Surf. Sci.* **600**, 3321–3326 (2006). <https://doi.org/10.1016/j.susc.2006.06.018>
- Li, H., Zhang, S., Zhou, S., Cao, X., Zheng, Y.: Crystalline size effect on the Energy transfer from Mo–O groups to Eu³⁺ ions in R₂MoO₆:Eu (R=La, Gd, and Y) crystals. *J. Phys. Chem. C.* **113**, 13115–13120 (2009). <https://doi.org/10.1021/jp903647v>
- Meena, M.L., Lu, C.-H., Som, S., Chaurasiya, R., Lin, S.D.: Highly efficient and thermally stable Eu³⁺ activated phosphate based phosphors for WLEDs: An experimental and DFT Study. *J. Alloys Compd.* **895**, 162670 (2022). <https://doi.org/10.1016/j.jallcom.2021.162670>
- Mehta, G.K.: Swift Heavy ions in materials Science—Emerging possibilities. *Vacuum*. **48**, 957–959 (1997). [https://doi.org/10.1016/S0042-207X\(97\)00102-4](https://doi.org/10.1016/S0042-207X(97)00102-4)
- Mishra, Y.K., Kabiraj, D., Avasthi, D.K., Pivin, J.C.: Swift Heavy Ion-Induced dissolution of gold nanoparticles in silica matrix. *Radiat. Eff. Defects Solids.* **162**, 207–213 (2007). <https://doi.org/10.1080/10420150601132883>
- Park, J.Y., Chung, J.W., Yang, H.K.: Versatile fluorescent Gd₂MoO₆:Eu³⁺ nanophosphor for latent fingerprints and anti-counterfeiting applications. *Ceram. Int.* **45**, 11591–11599 (2019). <https://doi.org/10.1016/j.ceramint.2019.03.030>
- Peña-Rodríguez, O., Olivares, J., Bányász, I.: Optical properties of Crystalline and Ion-Beam Amorphized Bi₁₂GeO₂₀: Relevance for Waveguide Applications. *Opt. Mater. (Amst)*. **47**, 328–332 (2015). <https://doi.org/10.1016/j.optmat.2015.05.050>
- Popov, A.I., Balanzat, E.F.: Centre Production in CsI and CsI–Tl crystals under Kr Ion Irradiation at 15 K. *Nucl. Instruments Methods Phys. Res. Sect. B Beam Interact. Mater. Atoms.* **166–167**, 545–549 (2000). [https://doi.org/10.1016/S0168-583X\(99\)00789-2](https://doi.org/10.1016/S0168-583X(99)00789-2)
- Ridgway, M.C., Giulian, R., Sprouster, D.J., Kluth, P., Araujo, L.L., Llewellyn, D.J., Byrne, A.P., Kremer, F., Fichtner, P.F.P., Rizza, G., et al.: Role of thermodynamics in the shape Transformation of embedded Metal nanoparticles Induced by Swift Heavy-Ion Irradiation. *Phys. Rev. Lett.* **106**, 95505 (2011). <https://doi.org/10.1103/PhysRevLett.106.095505>

- Som, S., Sharma, S.K., Lochab, S.P.: Morphology, Ion Impact, and kinetic parameters of Swift Heavy-Ion-Induced $Y_2O_3:Dy^{3+}$ phosphor. *Phys. Status Solidi*. **210**, 1624–1635 (2013). <https://doi.org/10.1002/pssa.201329197>
- Stoller, R.E., Toloczko, M.B., Was, G.S., Certain, A.G., Dwaraknath, S., Garner, F.A.: On the Use of SRIM for Computing Radiation damage exposure. *Nucl. Instruments Methods Phys. Res. Sect. B Beam Interact. Mater. Atoms*. **310**, 75–80 (2013). <https://doi.org/10.1016/j.nimb.2013.05.008>

Publisher's Note Springer Nature remains neutral with regard to jurisdictional claims in published maps and institutional affiliations.

Springer Nature or its licensor (e.g. a society or other partner) holds exclusive rights to this article under a publishing agreement with the author(s) or other rightsholder(s); author self-archiving of the accepted manuscript version of this article is solely governed by the terms of such publishing agreement and applicable law.

Authors and Affiliations

Somrita Dutta^{1,2} · Sudipta Som³ · Mohan Lal Meena⁴ · S. K. Sharma²

✉ Sudipta Som
sudiptasom@snuhennai.edu.in

Somrita Dutta
samy123bh@gmail.com

Mohan Lal Meena
mohan.meena78@gmail.com

S. K. Sharma
sksharma.iitism@gmail.com

¹ Department of Physics, National Taiwan Normal University, Taipei 10617, Taiwan, ROC

² Department of Applied Physics, Indian Institute of Technology (Indian School of Mines), Dhanbad 826004, India

³ Department of Physics, Shiv Nadar University Chennai, Chennai 603110, Tamil Nadu, India

⁴ Department of Chemical Engineering, National Institute of Technology Surathkal, Karnataka 575 025, India